

Kinetic frustration and the nature of the magnetic and paramagnetic states in iron pnictides and iron chalcogenides

Z. P. Yin^{1,2,*}, K. Haule¹, and G. Kotliar¹

¹*Department of Physics and Astronomy, Rutgers University, Piscataway, New Jersey 08854, United States. and*

²*Department of Physics and Astronomy, Stony Brook University, Stony Brook, New York 11794, United States.*

(Dated: November 26, 2024)

The iron pnictide and chalcogenide compounds are a subject of intensive investigations due to their high temperature superconductivity.[1] They all share the same structure, but there is significant variation in their physical properties, such as magnetic ordered moments, effective masses, superconducting gaps and T_c . Many theoretical techniques have been applied to individual compounds but no consistent description of the trends is available [2]. We carry out a comparative theoretical study of a large number of iron-based compounds in both their magnetic and paramagnetic states. We show that the nature of both states is well described by our method and the trends in all the calculated physical properties such as the ordered moments, effective masses and Fermi surfaces are in good agreement with experiments across the compounds. The variation of these properties can be traced to variations in the screening of the Coulomb interactions. Our results provide a natural explanation of the strongly Fermi surface dependent superconducting gaps observed in experiments[3]. We propose a specific optimization of the crystal structure to look for higher T_c superconductors.

The iron pnictides are Hund's metals [4], where the interaction between the electrons is not strong enough to fully localize them, but it significantly slows them down, so that the low energy quasiparticles have much enhanced mass. These quasiparticles are composites of charge and a fluctuating magnetic moment originating in the Hund's rule interactions which tend to align electrons with the same spin and different orbital quantum numbers when they find themselves on the same iron atom.

A central puzzle in this field is posed by the variation of the ordered magnetic moment across the iron pnictides/chalcogenides series. In the fully localized picture the atom resides in a single valence, therefore the ordered moment is equal to the atomic moment ($4\mu_B$ per iron), possibly reduced by quantum fluctuations. This picture is realized in cuprate superconductors where quantum fluctuations reduce the Cu^{2+} moment by 20%. In the fully itinerant weak coupling picture, such as spin density wave (SDW) in chromium metal, the ordered moment is related to the degree of Fermi surface nesting. It is by now clear that the iron pnictides are not well described by either fully localized or fully itinerant picture, nor by the density functional theory (DFT), which greatly overestimates the ordered magnetic

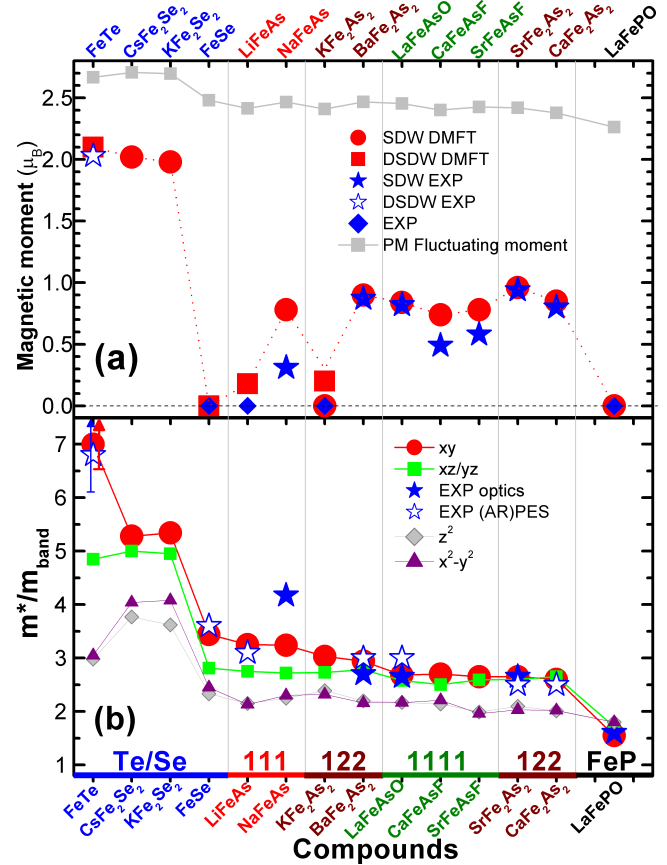


FIG. 1: **Ordered magnetic moments and mass enhancements in iron-based compounds.** (a) the DFT+DMFT calculated and experimental[6–13] Fe magnetic moments in the SDW and DSDW states. Also shown is the calculated fluctuating moment in the PM state. (b) The DFT+DMFT calculated mass enhancement m^*/m_{band} of the Fe 3d orbitals in the PM state and the low energy effective mass enhancement obtained from optical spectroscopy experiments[15–18] and (angle-resolved) photoemission spectroscopy experiments[19–24].

moments. It has been advocated that the shortcomings of DFT can be circumvented by incorporating the physics of long wavelength fluctuations [5]. Here we take the opposite perspective. While critical long-wavelength fluctuations certainly play a role near the phase transition lines, we will show that the local fluctuations on the iron atom can account for the correct trend of magnetic moments and correlation strength in iron pnictides/chalcogenide layered compounds.

Using the combination of density functional theory and dynamical mean field theory (DFT+DMFT) (see online ma-

terial for details), we studied two different real space orderings, the SDW ordering, characterized by wave vector $(\pi, 0, \pi)$ (this vector is written in coordinates with one Fe atom per unit cell), which is experimentally found in iron arsenide compounds, and $(\pi/2, \pi/2, \pi)$ ordering, denoted by double stripe spin density wave (DSDW). The latter was found experimentally in FeTe. Figure 1(a) shows our theoretical results for the ordered moment in both phases together with experimentally determined values [6–13] from across all known families of iron-based superconducting compounds. There is an overall good agreement between theory and experiment, in particular LaFePO is predicted to be nonmagnetic, the majority of 1111 and 122 compounds have ordered moment below $1.0 \mu_B$, and FeTe orders with DSDW moment of $2.1 \mu_B$.

We now explain the variation of the ordered moment in terms of real space and momentum space concepts. The size of the fluctuating local moment, which can be extracted from neutron scattering experiments, gives an upper bound to the size of the ordered magnetic moment and is also plotted in Fig. 1(a). It was computed from the atomic histogram displayed in Fig.2(c), which shows the percentage of time the iron $3d$ electrons spend in various atomic configurations when the system is still in its paramagnetic (PM) state. Only high spin states, which carry a large weight as a result of the Hund's rule coupling in iron, are displayed (see also online material for complete histogram). A monovalent histogram with only the atomic ground state would give iron magnetic moment of $4 \mu_B$.

In a correlated Fermi liquid, the spin excitations are described in terms of individual particle hole pair excitations and their collective motion. Their residual interaction can lead to a magnetic state when the particle hole excitations condense at non-zero wave vector. A large quasiparticle mass, naturally facilitates this condensation, hence we expect that the size of the ordered moment will correlate with the mass of the quasiparticles. In figure 1(b) we display separately the quasiparticle mass for all iron $3d$ orbitals in the PM state and we normalize it to its band value. Clearly there is some correlation between mass enhancement in Fig.1(b) and ordered magnetic moment in Fig.1(a) across various families of iron-based compounds. In particular, correlations are too weak for ordering in LaFePO, while very heavy quasiparticles in FeTe produce large moment of $2.1 \mu_B$. However, there are other factors presented below, such as kinetic frustration, orbital differentiation and Fermi surface shape, which together conspire to produce the magnetic orderings displayed in Fig.1(a).

The quasiparticle mass displayed in Fig. 1(b) is quite moderate in phosphorus 1111 compound on the right hand side of Fig.1(b), but correlations are significantly enhanced in arsenic 122 and 1111 compounds. Notice however, that enhancement is not equal in all orbitals, but it is significantly stronger in the $t2g$ orbitals, i.e., xz , yz , and xy . The correlations get even stronger in 111 compounds, such as LiFeAs and NaFeAs, and finally jump to significantly larger values of the order of five in selenides KFe_2Se_2 and CsFe_2Se_2 . Finally, the mass enhancement of the xy orbital

in FeTe exceeds factor of seven compared to the band mass, which is typical for heavy fermion materials, but is rarely found in transition metal compounds. We displayed only a lower bound for this mass as the end point of an arrow in Fig. 1(b), because the quasiparticles are not yet well formed at studied temperature $T=116$ K. Notice the strong orbital differentiation in FeTe, with xz/yz mass of five and eg mass enhancement of only three. This orbital differentiation signals that the material is in the vicinity of an orbital selective Mott transition, as proposed previously for other iron pnictides [14], where xy orbital is effectively insulating while other orbitals remain metallic. In Fig.1(b) we also display mass enhancement extracted from optics[15–18] and ARPES[19–24] measurements, and notice a good agreement between our theory and experiment when available. The effective mass extracted from ARPES and optics should be compared with that of the $t2g$ orbitals which contribute most of the spectral weight at low energy.

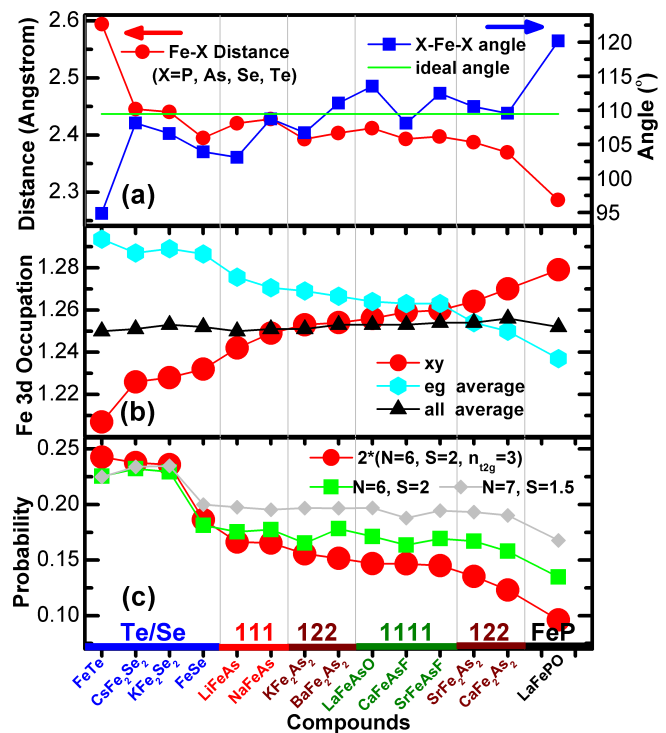


FIG. 2: **Structure, orbital occupation and probability of selected atomic states of Fe.** (a) The Fe-X ($X=P, \text{As}, \text{Se}$ and Te) distance and X-Fe-X angle in iron-based compounds, where the two X atoms are in the same ab plane. Note this angle is different from the X-Fe-X angle where the two X atoms are in different ab planes; (b) The orbital occupation of the xy orbital and the average values for the eg orbitals and all five orbitals; (c) The probability of selected atomic configurations of Fe where N (S) is the total number (spin) of Fe $3d$ electrons in the atomic configuration.

The large mass enhancement in Hund's metals is due to an orbital blocking mechanism. If the Hund's coupling is very large, only the high spin states have a finite probability in atomic histogram. The atomic high spin ground state has maximum possible spin $S = 2$, and is orbitally a sin-

glet, which does not allow mixing of the orbitals and leads to orbital blocking, i.e., $\langle gs|d_{\alpha}^{\dagger}d_{\beta}|gs\rangle = 0$ when $\alpha \neq \beta$, where $|gs\rangle$ is the atomic ground state in the $3d^6$ configuration, and α is the iron orbital index. In the localized limit and in the absence of crystal field effects, it is possible to derive a low energy effective Kondo model, which has Kondo coupling for factor of $(2S+1)^2$ smaller than a model without Hund's coupling [25]. Since the Kondo temperature T_K depends on the Kondo coupling I_0 exponentially ($T_K \propto \exp(-1/I_0)$), this results in enormous mass enhancement of the order of $\exp(((2S+1)^2 - 1)/I_0)$ compared to the system with negligible Hund's coupling (see also online material).

Having established why heavy quasiparticles form in iron pnictides and chalcogenides, we can now study how the key parameters of the crystal structure control the strength of correlations and other physical properties, keeping the same on-site Coulomb interaction matrix. The iron-pnictogen distance, displayed in Fig. 2(a), controls the overlap between iron and pnictogen atom and hence makes iron electrons more localized (itinerant) with increasing (decreasing) distance. The largest distance is achieved in compounds with larger chalcogenide ion, such as in FeTe, which results in very heavy quasiparticles, as seen in Fig. 1(b). The variation in distance alters the overall bandwidth moderately. The Hund's orbital blocking mechanism amplifies this variation.

The second key structural parameter is the tetrahedron shape, which is parameterized in terms of pnictogen-Fe-pnictogen angle, displayed in Fig. 2(a). This angle is equal to 109.5° for an ideal tetrahedron, and is much smaller in FeTe, where the Te ion is pushed further away from Fe plane. The shape of the tetrahedron controls the crystal field levels, which in turn control the orbital occupancies. We display them in Fig. 2(b). The average occupation of iron atom is around $n_d = 6.25$ across all the compounds studied, which leads to an average orbital occupation of $n_{\alpha} = 1.25$. A deviation from ideal angle enhances the crystal field splittings between xy and the degenerate xz/yz orbital and also changes the splitting between $t2g$ and eg orbitals. Heavier quasiparticles with smaller quasiparticle bandwidth are more susceptible to the crystal field splitting, hence the orbital differentiation is largest in FeTe but very small in LaFePO. The net result of crystal field splittings and quasiparticle mass is the charge transfer from the $t2g$ to eg orbitals as seen in Fig. 2(b), and among $t2g$'s the xy orbital loses most charge with increased correlation strength, pushing its occupancy closer to integer filling.

Furthermore, the effective hopping between neighboring iron atoms has two contributions, one is due to direct iron-iron overlap, and the second is indirect hop through pnictogen atom. The two contributions to the diagonal hopping $t_{\alpha,\alpha}$ have *opposite* sign and destructively interfere. For the xz and yz orbital, the indirect hopping through pnictogen is larger than direct iron-iron hop. For the xy orbital, the two contributions are very similar, and when the pnictogen height is sufficiently large, such as in FeTe, the indirect hop is reduced and the two contributions almost exactly cancel each other, resulting in vanishing effective nearest neighbor

iron-iron $t_{xy,xy}$ hopping. This kinetic frustration mechanism contributes to the dramatic enhancement of the xy mass in the FeTe compound.

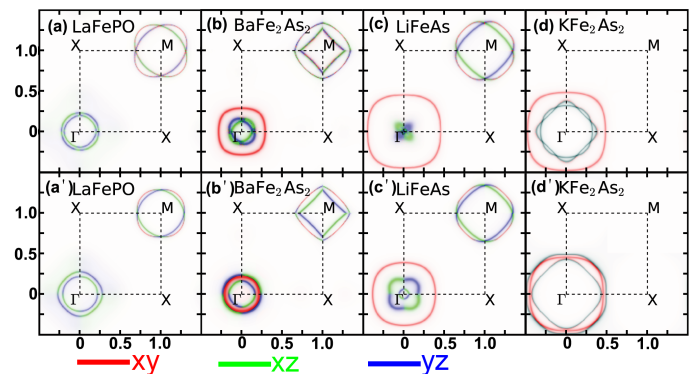


FIG. 3: **Fermi surface.** The DFT+DMFT (top row) and DFT (bottom row) calculated 2D Fermi surface in the Γ plane ($k_z = 0$) for (a)LaFePO; (b)BaFe₂As₂; (c)LiFeAs; (d)KFe₂As₂. The Fermi surface is colored in red, green and blue according to its orbital character of xy , xz and yz , respectively.

In itinerant systems, the shape of the Fermi surface, or the Fermi surface nesting is relevant for deciding which magnetic ordering wave vector is realized when the residual interactions among the quasiparticles is sufficiently strong. Additional terms, arising from the incoherent part of the electron become increasingly important as the localization threshold is approached.

In Fig. 3 we display DFT+DMFT Fermi surface together with DFT predictions. In the moderately correlated end, such as in the phosphorus 1111 compounds, our theoretical predictions match DFT results. However, when correlations become sizable, such as in LaFeAsO or BaFe₂As₂, the xy orbital starts to play a special role, which results in slightly modified Fermi surface shape and character compared with DFT, while respecting the Luttinger theorem. In BaFe₂As₂ DFT predicts that the outer pocket at Γ is of xz/yz character, while DFT+DMFT predicts that the outer pocket is of xy character, in agreement with experiments [26]. This effect of growing xy pocket at Γ and consequently shrinking of xz/yz pocket is even more apparent in LiFeAs. In the latter compound DFT also predicts the outer pocket to be of xy character, but its size is considerably smaller than measured in ARPES experiment [21]. DFT+DMFT increased size of the outer xy pocket together with the butterfly shape of the xz/yz pocket at Γ are in good agreement with experiment of Ref.21. These changes in the shape of the Fermi surfaces are the momentum space counterpart of the real space picture of charge transfer among the iron $3d$ orbitals shown in Fig. 2(b). This is because the decrease (increase) of the xy (xz, yz) orbital occupancy results in the increase (decrease) of the hole pocket size. Finally, the Fermi surface of KFe₂As₂ displayed in Fig. 3 has only hole pockets around Γ but no electron pockets at M , hence there is no Fermi surface nesting to facilitate the long range magnetic order. Indeed KFe₂As₂ can not sustain SDW ordering and only a tiny DSDW moment can be stabilized, as shown in

Fig. 1(a). Even though the mass enhancement in KFe_2As_2 and 111 compounds is substantial, the Fermi surface nesting still plays an important role in stabilizing magnetic ordering.

The fluctuating moment presented in Fig. 1(a) monotonically increases with increased correlation strength, and constitutes an upper bound to the size of the ordered magnetic moment. However, even when the Fermi surface nesting is quite good, such as in 1111 and many 122 compounds, the ordered moment is substantially reduced from this upper bound. A part of the reduction is due to kinetic frustration, discussed above. This effect is properly treated by DFT method, nevertheless the ordered moment predicted by DFT is around $2.0 \mu_B$ (see also online material), substantially above the experimentally measured values. In the DFT+DMFT theoretical method, the orbital differentiation is responsible for large overall reduction of the static moment. In very itinerant system, such as LaFePO , the quasiparticles are too weakly interacting to condense, hence moderate correlations with mass enhancement of 1.5 do not sufficiently localize electrons to allow magnetic ordering. In most of other compounds, the localization and hence the effective mass increase is substantial only in $t2g$ orbitals, while eg orbitals remain only moderately correlated. Consequently the ordered magnetic moment is small in eg orbitals, which causes only a fraction of the fluctuating moment to order. Only when correlations are very strong and equal in all orbitals, almost the entire fluctuating moment orders. Such an example is provided by $\text{K}_{0.8}\text{Fe}_{1.6}\text{Se}_2$, which is obtained by introducing iron vacancies into KFe_2Se_2 , where the entire fluctuating moment of $3.3\mu_B$ orders. [27]

We conclude with some experimental consequences of the theory. We established that in compounds with substantial mass enhancement, the xy orbital is the heaviest and most incoherent, placing FeTe at the verge of an orbitally selective Mott transition. Furthermore we have identified the chemical handle, kinetic frustration, responsible for this effect. This idea can be tested by applying uniaxial pressure on the FeTe , which should result in a noticeable restoration of coherence in the transport properties. Our results also suggest a natural origin for a *particle-hole asymmetry* in doping the parent compounds. Reducing the iron occupancy of the $3d$ orbital, brings the occupancy of the xy orbital closer to unity, and increases the correlation strength, which in turn strengthens the magnetic moment. This has been observed in ARPES studies of the BaFe_2As_2 family[28].

In the magnetic state, the in-plane resistivity is very anisotropic, as has been shown in optical and transport studies of BaFe_2As_2 [29, 30]. This is a consequence of the strong low energy orbital polarization of the xz and yz orbital[30]. Increased correlation strength results in an increasing participation of the xy orbital, with magnetic moment concentrated in the xy orbital, which does not cause the in-plane polarization. Hence, in-plane transport and optical anisotropy should be reduced with increase of correlation strength and orbital differentiation.

Our work suggests that larger mass enhancement of the xy orbital leads to smaller superconducting gap on the most

outside hole pocket centered at Γ , which is mostly of xy character. Furthermore, large degeneracy is a fertile ground for superconductivity, while large orbital differentiation is harmful, which suggests that superconductivity is hard to achieve when $X\text{-Fe-X}$ angle is small. On the other hand, large $X\text{-Fe-X}$ angle in iron pnictides and chalcogenides is accompanied by small $X\text{-Fe}$ distance, which weakens magnetism and hence likely undermines superconducting pairing strength. We thus suggest that good candidates for high temperature superconductivity are compounds with $X\text{-Fe-X}$ angle close to ideal angle, as observed by Lee *et al.*[31] in order to achieve small orbital differentiation, but with the largest possible $X\text{-Fe}$ distance to strengthen spin fluctuations.

METHOD

We use fixed Coulomb interaction parameters for all materials in our DFT+DMFT calculations in order to keep parameter-free spirit and to demonstrate that the variations in the calculated physical properties is mainly due to the variations in the key structural parameters, rather than changes in the screening of the Coulomb interactions. The detail of the method is included in online material.

* Electronic address: yinzping@physics.rutgers.edu

- [1] Kamihara, Y. *et al.* Iron-based layered superconductor $\text{La}[\text{O}_{1-x}\text{F}_x]\text{FeAs}$ ($x = 0.05\text{-}0.12$) with $T_c = 26$ K. *J. Amer. Chem. Soc.* **130**, 3296-3297 (2008).
- [2] Paglione, J. & Greene, R. L. High-temperature superconductivity in iron-based materials. *Nat. Phys.* **6**, 645-658 (2010).
- [3] Ding, H. *et al.* Observation of Fermi-surface-dependent nodeless superconducting gaps in $\text{Ba}_{0.6}\text{K}_{0.4}\text{Fe}_2\text{As}_2$. *EPL* **83**, 47001 (2008).
- [4] Haule, K. & Kotliar, G. Coherence-incoherence crossover in the normal state of iron-oxypnictides and importance of the Hund's rule coupling. *New J. Phys.* **11**, 025021 (2009).
- [5] Mazin, I. I & Johannes, M. D. A key role for unusual spin dynamics in ferropnictides. *Nat. Phys.* **5**, 141-145 (2009).
- [6] Bao, W. *et al.* Incommensurate magnetic order in the $\alpha\text{-Fe}(\text{Te},\text{Se})$ superconductor systems. *Phys. Rev. Lett.* **102**, 247001 (2009).
- [7] Yu, W. Q. *et al.* ^{23}Na and ^{75}As NMR study of antiferromagnetism and spin fluctuations on NaFeAs single crystals. Arxiv:1004.3581.
- [8] Huang, Q. *et al.* Magnetic order in BaFe_2As_2 , the parent compound of the FeAs based superconductors in a new structural family. *Phys. Rev. Lett.* **101**, 257003 (2008).
- [9] Li, H.-F. *et al.* Phase transitions and iron-ordered moment form factor in LaFeAsO . *Phys. Rev. B* **82**, 064409 (2010).
- [10] Xiao, Y. *et al.* Magnetic order in $\text{CaFe}_{1-x}\text{Co}_x\text{AsF}$ ($x = 0, 0.06, 0.12$) superconductor compounds. *Phys. Rev. B* **79**, 060504(R) (2009).
- [11] Xiao, Y. *et al.* Neutron diffraction study on phase transition and thermal expansion of SrFeAsF . *Phys. Rev. B* **81**, 094523 (2010).
- [12] Zhao, J. *et al.* Spin and lattice structure of single crystal SrFe_2As_2 . *Phys. Rev. B* **78**, 140504(R) (2008).
- [13] Goldman, A. I. *et al.* Lattice and magnetic instabilities in CaFe_2As_2 : a single crystal neutron diffraction study. *Phys. Rev. B* **78**, 100506(R) (2008).

- [14] de' Medici, L. *et al.* Orbital-selective Mott transition out of band degeneracy lifting. *Phys. Rev. Lett.* **102**, 126401 (2009).
- [15] Hu, W. Z. *et al.* Optical study on the spin-density wave properties in single crystalline $\text{Na}_{1-\delta}\text{FeAs}$. *Phys. Rev. B* **80**, 100507(R) (2009).
- [16] Hu, W. Z. *et al.* Origin of the spin density wave instability in AFe_2As_2 (A=Ba, Sr) as revealed by optical spectroscopy. *Phys. Rev. Lett.* **101**, 257005 (2008).
- [17] Chen, Z. G. *et al.* Optical spectroscopy study on single crystalline LaFeAsO . *Phys. Rev. B* **81**, 100502(R) (2010).
- [18] Qazilbash, M. M. *et al.* Electronic correlations in the iron pnictides. *Nat. Phys.* **5**, 647-650 (2009).
- [19] Tamai, A. *et al.* Strong electron correlations in the normal state of $\text{FeSe}_{0.42}\text{Te}_{0.58}$. *Phys. Rev. Lett.* **104**, 097002 (2010).
- [20] Yamasaki, A. *et al.* Electron correlation in FeSe superconductor studied by bulk-sensitive photoemission spectroscopy. *Phys. Rev. B* **82**, 184511 (2010).
- [21] Borisenko, S. V. *et al.* Superconductivity without magnetism in LiFeAs . *Phys. Rev. Lett.* **105**, 067002 (2010).
- [22] Yi, M. *et al.* Unconventional electronic reconstruction in undoped $(\text{Ba,Sr})\text{Fe}_2\text{As}_2$ across the spin density wave transition. *Phys. Rev. B* **80**, 174510 (2009).
- [23] Kim, Y. K. *et al.* Electronic structure studies of detwinned BaFe_2As_2 by photoemission. Arxiv:1011.1112.
- [24] Wang, Q. *et al.* Uniaxial “nematic-like” electronic structure and Fermi surface of untwinned CaFe_2As_2 . Arxiv:1009.0271.
- [25] Okada, I. & Yosida, K. Singlet ground state of the localized d -electrons coupled with conduction electrons in metals. *Progress of Theoretical Physics* **49**, 1483-1502 (1973).
- [26] Zhang, Y. *et al.* Orbital characters of bands in iron-based superconductor $\text{BaFe}_{1.85}\text{Co}_{0.15}\text{As}_2$. *Phys. Rev. B* **83**, 054510 (2011).
- [27] Yin, Z. P., Haule, K. & Kotliar G. manuscript in preparation (2011).
- [28] Yi, M. *et al.* Electronic structure of the BaFe_2As_2 family of iron-pnictide superconductors. *Phys. Rev. B* **80**, 024515 (2009).
- [29] Dusza, A. *et al.* Anisotropic charge dynamics in detwinned $\text{Ba}(\text{Fe}_{1-x}\text{Co}_x)_2\text{As}_2$. *EPL* **93**, 37002 (2011).
- [30] Yin, Z. P., Haule, K. & Kotliar, G. Magnetism and charge dynamics in iron pnictides. *Nat. Phys.* **7**, 294-297 (2011).
- [31] Lee, C.-H. *et al.* Effect of structural parameters on superconductivity in fluorine-free LnFeAsO_{1-y} ($\text{Ln} = \text{La}, \text{Nd}$). *J. Phys. Soc. Jpn.* **77**, 083704 (2008).

Acknowledgments ZPY and GK were supported by NSF DMR-0906943, KH was supported by NSF DMR-0746395. Part of the work (ZPY) was carried out under the auspices of a DoD National Security Science and Engineering Faculty Fellowship, via AFOSR grant FA 9550-10-1-0191. Acknowledgment (KH) is made to the donors of the American Chemical Society Petroleum Research Fund for partial support of this research.

Kinetic frustration and the nature of the magnetic and paramagnetic states in iron pnictides and iron chalcogenides: Supplementary online material

Z. P. Yin^{1,2}, K. Haule¹, and G. Kotliar¹

¹*Department of Physics and Astronomy, Rutgers University, Piscataway, New Jersey 08854, United States.*

²*Department of Physics and Astronomy, Stony Brook University, Stony Brook, New York 11794, United States.*

Method

We use the combination of density functional theory and dynamical mean field theory (DFT+DMFT) [S1] as implemented in Ref. S2, which is based on the full-potential linear augmented plane wave method implemented in Wien2K [S3], to carry out our first principles calculations. The electronic charge is computed self-consistently on DFT+DMFT density matrix. The quantum impurity problem is solved by the continuous time quantum Monte Carlo method [S4, S5], using Slater form of the Coulomb repulsion in its fully rotational invariant form.

We use the experimentally determined lattice structures, including the internal positions of the atoms, from Refs. [S6 - S19]. We use the paramagnetic tetragonal lattice structures, and neglect the weak structural distortions. This distortion has a very small effect on the size of the magnetic moment, proving that the magnetism has electronic rather than structural origin.

We studied the paramagnetic phase of all compounds at the same temperature of $T = 116$ K, and magnetic states (SDW and DSDW) at $T = 72.5$ K. Our *ab initio* estimation for the Coulomb interaction U and Hund's coupling J in BaFe_2As_2 are $U = 5.0$ eV and $J = 0.8$ eV [S20]. We checked that the Hund's coupling, which is very weakly screened in solids, is very similar in other compounds, such as FeTe, where it increases for less than 5% compared to BaFe_2As_2 . As shown in Ref. [S21], physical properties are not sensitive to small variation of Hubbard interaction U , hence we fixed Coulomb interaction U and J to the same *ab initio* determined values ($U = 5.0$ eV and $J = 0.8$ eV) across all studied compounds in the paramagnetic phase and DSDW phase, whereas a fixed $U = 5.0$ eV and a smaller fixed $J = 0.7$ eV are used in the SDW state in consistent with our previous calculations for BaFe_2As_2 in the SDW phase.[S21]

Histograms and Density of States

To analyze the character of the many body wave function, it is instructive to project it to momentum and real space basis. The one electron spectral function contains the information of the overlap between the many body wave function and the plane wave basis. It is also instructive to project the wave function to the atomic basis on the iron site. This projection can be presented in the form of the atomic histogram. In any given period of time, an iron atom visits many states from the atomic basis on the timescale, which is proportional to the quasiparticle mass enhancement. The probability to find an iron atom in the solid in one of the atomic states, is called the atomic his-

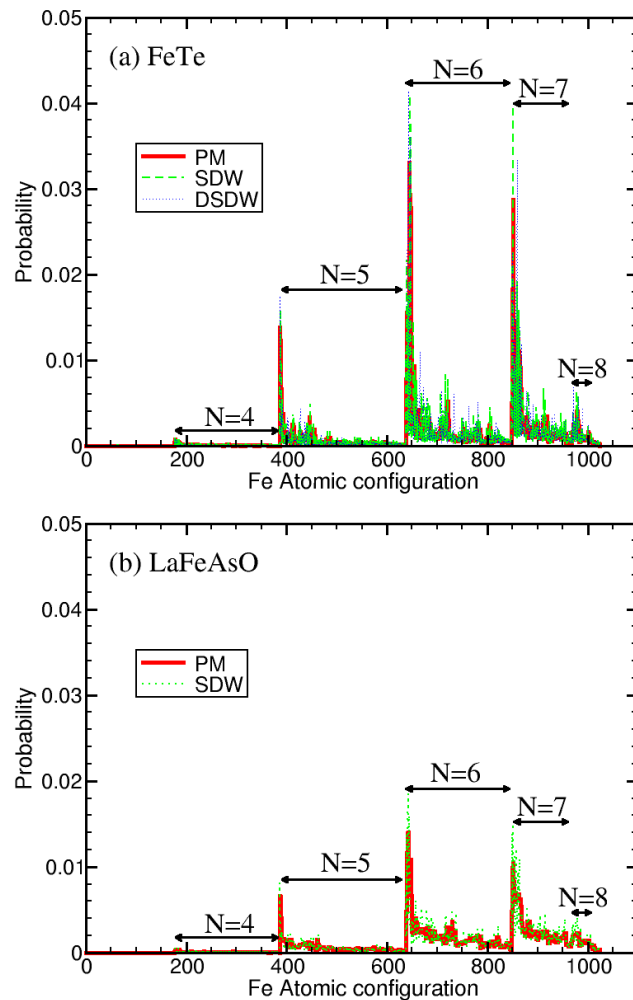


FIG. S1: **Atomic histogram** The atomic histogram of the Fe-3d shell for (a) FeTe and (b) LaFeAsO in the paramagnetic state and magnetic states. The 1024 possible atomic configurations are sorted by the number of 3d electrons of the individual configuration.

togram, and a typical example is provided in Fig. S1. Here the atomic basis is constructed from the five 3d orbitals of an iron atom, which together with spin, span a Hilbert space of size $2^{10} = 1024$. We sort these states first according to their occupancy $N = 0, 1, \dots, 10$, and within the same occupancy, we sort them according to their atomic energy. Due to large Hund's coupling the first (last) few states at given N are the high (low) spin states. In Fig. S1 we clearly see the spikes in probability for the high spin states (at the beginning of the constant N interval). Consequently, the low spin states (at the end of the constant N interval) lose substantial weight. In the absence of Hund's coupling, the

high and the low spin states would be equally probable. We plot in Fig. S1 two representative histograms, for FeTe and LaFeAsO compounds. The two histograms are qualitatively similar, nevertheless the differentiation between the high-spin states and the low spin states in FeTe is more amplified. In the magnetic states such as SDW and DSDW states, the high spin atomic states gain even more weight, as seen in Fig. S1.

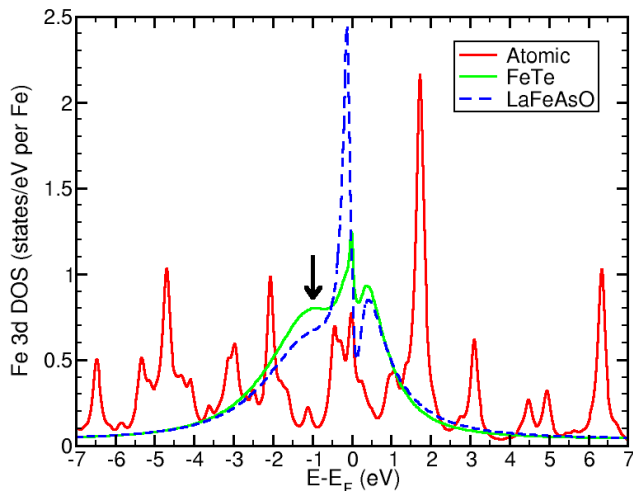


FIG. S2: **Fe 3d DOS** Atomic-like Fe 3d DOS for FeTe contrasted with actual Fe 3d DOS of LaFeAsO and FeTe computed by DFT+DMFT.

The valence histogram of a Hund’s metal is fundamentally different from that of an oxide. While only a few atomic states have a significant probability in an oxide, Hund’s metals visit a large number of atomic states over time, resulting in a dramatic (40%) reduction of the magnetic moment due to valence fluctuations. A monovalent histogram with only the atomic ground state would give iron magnetic moment of $4 \mu_B$.

Another interesting feature of Hund’s metals is that very large number of atomic states has finite probability. For comparison, in transition metal oxides or in heavy fermion materials with similar mass enhancement as in iron pnictides and chalcogenides, the atomic histogram would contain only a small number of states with significant probability [S22]. Since the Hund’s rule coupling J is equal to 0.8 eV , the energy spread of atomic states at constant $N = 5$ or $N = 6$ is very large, of the order of $6 - 7 \text{ eV}$. Because there are many atomic states with finite probability that contribute to the one electron spectral function, and because those states are extended over a wide energy range, the spectral function does not have a very well defined atomic like excitations. To demonstrate this effect, we plot in Fig. S2(a) an atomic spectral function of Fe 3d orbitals, obtained from the corresponding atomic Green’s function defined by

$$G(\omega) = \sum_{\alpha, m, n} \frac{|\langle n | d_{\alpha}^{\dagger} | m \rangle|^2 (P_n + P_m)}{\omega - E_n + E_m} \quad (1)$$

where n, m run over all atomic states, and α runs over Fe

3d orbitals, and P_n are atomic probabilities displayed in Fig. S1. Clearly, the atomic spectral weight is distributed over a very large energy range. For comparison, a typical heavy fermion would have one sharp peak (a delta function) below the Fermi level, and another peak above the Fermi level, i.e., a lower and an upper Hubbard band.[S22]

In Fig. S2(a) we also show the full DFT+DMFT spectral function of the iron atom in the solid for FeTe and LaFeAsO. One can notice that these spectral functions have a sharp quasiparticle peak close to the Fermi level. Due to larger mass enhancement in FeTe, the quasiparticle peak in this compound is substantially smaller than in LaFeAsO. The rest of the spectral weight does not have a well defined Hubbard like bands, not because the rest of the spectra would be coherent, but because of the unusual atomic histograms of the Hund’s metals. A small feature around -2 to -1 eV is however noticeably enhanced in FeTe compared to LaFeAsO. This peak was identified in Ref. S23 as an atomic-like excitation, which is found in atomic spectral function at -2.2 eV , and is related to the excitation from atomic ground state of d^6 to atomic ground state of d^5 .

In the manuscript, we showed that one important factor in determining the size of the magnetic moment is the quasiparticle mass enhancement. Clearly the heavier quasiparticles with smaller quasiparticle effective width are more prone to ordering. It is interesting to inspect also the “quasiparticle height”, i.e., the value of the one-electron spectral function at the Fermi level. In Stoner theory, this value plays a crucial role in determining the critical temperature and the size of the ordered moment. In Fig. S3(a) we show the value of the density of states at the Fermi level in the paramagnetic state as obtained by both DFT and DFT+DMFT. Clearly, large density of states at the Fermi level is more compatible with the small moment rather than large moment (shown in Fig. S3(b)), which disfavors Stoner theory for explanation of the trends in magnetic states across iron pnictides and chalcogenides.

We also show in Fig. S3(b) the magnetic moment in the SDW and DSDW phases calculated by DFT with both the local spin density approximation (LSDA[S24]) and generalized gradient approximation (GGA[S25]) exchange correlation functionals. We also repeat the paramagnetic fluctuating moment and the experimental static ordered moments from the manuscript for better comparison. It is clear from Fig. S3(b) that the DFT calculated magnetic moments roughly follows the trend of the fluctuating moment in the PM state, but is very different from the static ordered moment, as already pointed out by Ref. S26.

Optical properties

Now we turn to the plasma frequencies in the paramagnetic state of iron pnictide and chalcogenide compounds, shown in Fig. S4. We show separately the in-plane and c-axis values, as obtained by both the DFT+DMFT and DFT calculations. We also plot the experimentally determined in-plane values from Refs. [S27] for $\text{Na}_{1-\delta}\text{FeAs}$, [S28] for

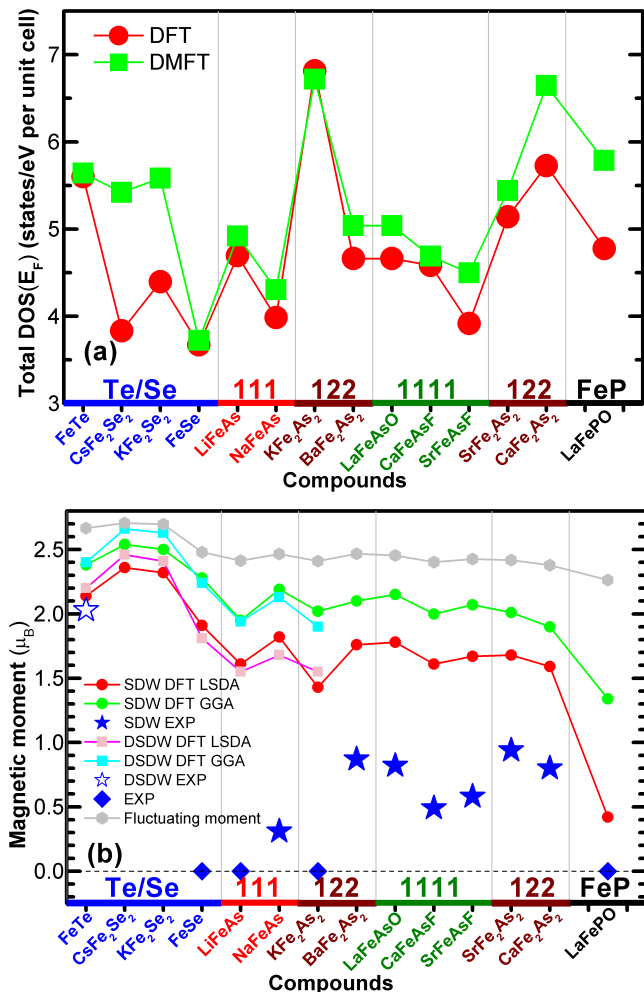


FIG. S3: **DOS and magnetic moment:** (a) Total density of states at the Fermi level in the PM phase computed by DFT and DFT+DMFT. (b) The magnetic moment calculated by DFT with both LSDA and GGA exchange-correlation functionals in both the SDW phase and DSDW phase. The fluctuating moment in the PM phase calculated by DFT+DMFT and the experimental magnetic moment in the magnetic states which are shown in Fig1(a) in the manuscript and reproduced here for easier comparison.

BaFe₂As₂ and SrFe₂As₂, [S29] for LaFeAsO, and [S30] for LaFePO. The DFT+DMFT calculated in-plane plasma frequencies agree well with existing optical measurements, but are significantly reduced from the DFT values, showing the important of correlation effect. The extracted plasma frequencies in the DFT+DMFT calculation for FeTe are most strongly reduced from DFT values, and bear bigger error bars due to the fact that the scattering rate in FeTe is so large that there is no well defined Drude peak in the optical conductivity. The c -axis Drude response is not very different from the DFT prediction, which can be rationalized by the fact that mass enhancement for the z^2 orbital is the smallest.

In Fig. S4 we also plot the inverse of the interlayer distance c^* of the Fe planes, multiplied by a constant factor, i.e., $12/c^*$. There is clearly a correlation between the inverse

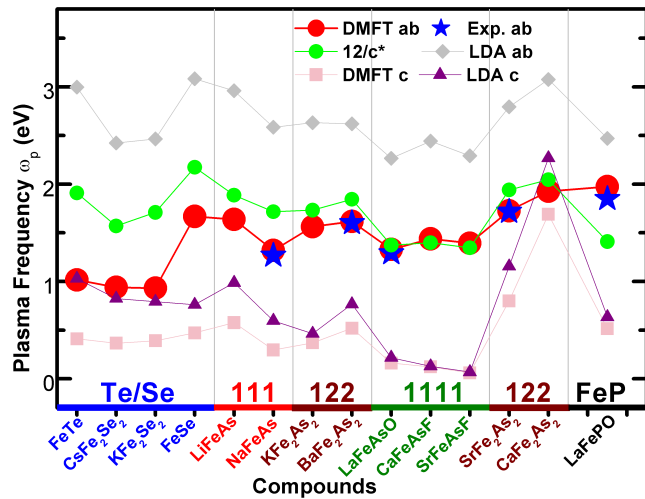


FIG. S4: **Plasma frequency.** The PM in-plane plasma frequency ω_{ab} and out-of-plane plasma frequency ω_c for various iron pnictides and iron chalcogenides calculated by both DFT+DMFT and DFT. The experimental PM in-plane plasma frequencies are taken from Refs. S27 - S30.

of the interlayer distance and in-plane Drude peak strength, suggesting that crystal structure again plays the key role in optical response.

Orbital blocking mechanism

As explained in the manuscript, the orbital blocking mechanism dramatically increases the strength of correlations in some multiorbital systems with large Hund's coupling, when the atomic ground state has large spin S .

To understand this mechanism in terms of mathematical equations, it is useful to translate the multiorbital system to the language of a self consistent Kondo effect [S31], describing the formation of composite quasiparticles via a Kondo Hamiltonian having a form $\sum_{k,k',\alpha,\beta} I_{\alpha,\beta} d_{\alpha\sigma}^\dagger d_{\beta\sigma'} c_{k'\beta,\sigma'}^\dagger c_{k\alpha,\sigma}$ plus the band Hamiltonian of free electrons and the impurity Hund's term. The Kondo interaction is given by $I_{\alpha,\beta} = \langle d_{\alpha}^\dagger \frac{1}{H} d_{\beta} \rangle + c.c.$ with H an effective atomic Hamiltonian and $\langle \rangle$ an average of the most probable atomic configurations [S31]. In the limit of no Hund's coupling, the Kondo coupling I is independent of orbital indices and the characteristic coherence scale is given by $T_K \propto \exp(-1/(IN\rho))$ where $N = 2S + 1$ is the orbital degeneracy. In the limit of large Hund's coupling, the impurity is represented by a maximal spin S , and the $I_{\alpha,\beta}$ is diagonal, since the Hund's rule coupling jams electrons into the same spin and different orbital one particle states in the low energy many body state. As a result, the Kondo energy is dramatically reduced to $T_K \propto \exp(-N/(I\rho))$ [S32]. We clearly see that the Hund's rule coupling has a strong effect in reducing the coherence scale.

The crystal field splittings regulate the orbital selectivity of the mass enhancement via the orbital selective blocking mechanism. The more diagonal the effective Kondo cou-

pling, the stronger the correlations. There are two types of high spin states in atomic $3d^6$ configurations, namely $eg^3t_2g^3$ and $eg^2t_2g^4$. When the low energy atomic configuration is $eg^3t_2g^3$ ($eg^2t_2g^4$), the t_2g (eg) orbitals remain blocked, while eg (t_2g) orbitals can mix. From this consideration it is clear that the crystal field environment which puts eg orbitals below t_2g makes the $eg^3t_2g^3$ primary configuration, and effectively blocks the t_2g orbitals, causing substantially larger effective mass for t_2g orbitals. This crystal field sequence is realized in most of compounds we studied. The only exception is LaFePO, in which eg states are slightly above t_2g , leading to slightly stronger correlations in eg orbitals.

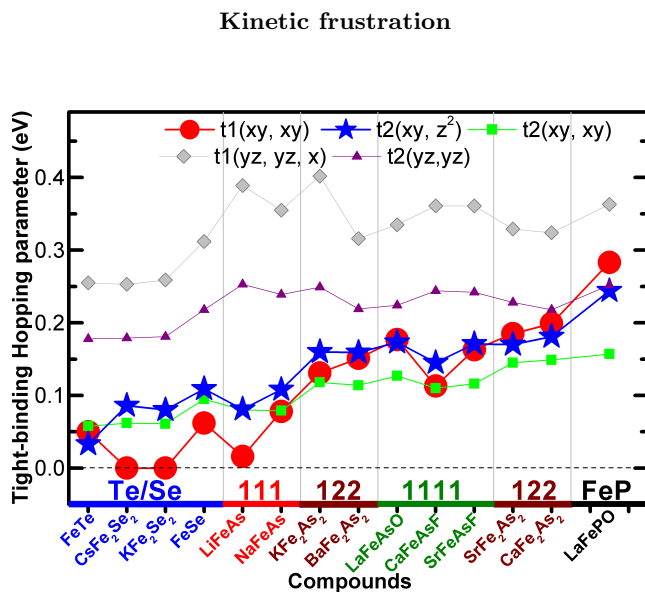


FIG. S5: **Hopping parameters** The hopping parameters of xy and yz orbitals to some selected orbitals of their nearest neighbor and next nearest neighbor Fe atoms obtained from tight-binding downfolding the DFT bands of the PM phase.

To gain some insights into the low energy physics of iron pnictide and chalcogenide compounds, we also constructed a low energy effective tight-binding model. This postprocessing step is here used to understand why a relatively small change in crystal structure can lead to enormous difference in mass enhancement. When the model contains both the iron d electrons and pnictide/chalcogenide p electrons, the hopping parameters do not show any anomalies or specific trend which could explain the variation of masses. On the other hand, the effective model which contains iron d electrons only, gives a clear signature that the hopping of the electrons on the iron xy orbital is severely impeded on the more correlated end, from LiFeAs towards FeTe. These hoppings are displayed in Fig. S5.

From geometrical considerations, it is clear that direct iron $d_{xy} - d_{xy}$ overlap between two neighboring atoms is always negative. This is due to the sign alternation of the wave function on the lobes of a d_{xy} orbital. On the other hand, the indirect hopping through pnictogen atom p or-

bitals such as p_x , is positive. While the indirect hopping through pnictogen p orbitals is larger than direct hopping for xz and yz orbitals, this contribution is comparable for the xy orbital. When pnictogen height increases, the indirect hopping decreases, and almost exactly cancels the direct hopping, resulting in negligible effective low energy $xy - xy$ hopping, hence $t1(xy, xy)$ in Fig. S5 becomes vanishingly small in the FeTe end. It is important to note that the bandwidth of the xy orbital does not change very dramatically, because the off-diagonal hopping $t1(xy, xz)$ remains large (0.22-0.24 eV) even in correlated compounds. Nevertheless, the most important diagonal hopping $t1(xy, xy)$ dramatically decrease together with the next nearest neighbor $t2(xy, xy)$ and off diagonal next nearest neighbor $t2(xy, z^2)$ hopping. Due to this kinetic frustration mechanism the diagonal hopping is small in correlated compounds such as FeTe. Due to orbital blocking mechanism, the mixing of the orbitals is blocked, and hence the correlations can increase dramatically in the xy orbital.

* Electronic address: yinzping@physics.rutgers.edu

- [S1] Kotliar, G., Savrasov, S. Y., Haule, K., Oudovenko, V. S., Parcollet, O. & Marianetti, C. A. Electronic structure calculations with dynamical mean-field theory. *Rev. Mod. Phys.* **78**, 865-951 (2006).
- [S2] Haule, K., Yee, C.-H. & Kim, K. Dynamical mean-field theory within the full-potential methods: electronic structure of CeIrIn₅, CeCoIn₅, and CeRhIn₅. *Phys. Rev. B* **81**, 195107 (2010).
- [S3] Blaha, P., Schwarz, K., Madsen, G. K. H., Kvasnicka, D. & Luitz, J. WIEN2K An augmented plane wave + local orbitals program for calculating crystal properties, (K. Schwarz, Techn. Univ. Wien, Austria, 2001).
- [S4] Haule, K. Quantum Monte Carlo impurity solver for cluster dynamical mean-field theory and electronic structure calculations with adjustable cluster base. *Phys. Rev. B* **75**, 151113 (2007).
- [S5] Werner, P., Comanac, A., de Medici, L., Troyer, M. & Millis, A. J. Continuous-time solver for quantum impurity models. *Phys. Rev. Lett.* **97**, 076405 (2006).
- [S6] Tropeano, M., Pallechi, I., Cimberle, M. R., Ferdeghini, C., Lamura, G., Vignolo, A., Martinelli, A., Palenzona, A. & Putti, M. Transport and superconducting properties of Fe-based superconductors: SmFeAs(O_{1-x}F_x) versus Fe_{1+y}(Te_{1-x}Se_x). *Supercond. Sci. Technol.* **23**, 054001 (2010).
- [S7] Krzton-Maziopa, A., Shermadini, Z., Pomjakushina, E., Pomjakushin, V., Bendele, M., Amato, A., Khasanov, R., Luetkens, H., & Conder, K. Synthesis and crystal growth of Cs_{0.8}(FeSe_{0.98})₂: a new iron-based superconductor with T_c=27K. *J. Phys. Condens. Matter* **23**, 052203 (2011).
- [S8] Guo, J. G., Jin, S. F., Wang, G., Wang, S. C., Zhu, K. X., Zhou, T. T., He, M. & Chen, X. L. Superconductivity in the iron selenide K_xFe₂Se₂ (0 ≤ x ≤ 1.0). *Phys. Rev. B* **82**, 180520(R) (2010).
- [S9] Phelan, D., Millican, J. N., Thomas, E. L., Leao, J. B., Qiu, Y. & Paul, P. Neutron scattering Measurements of the phonon density of states of FeSe_{1-x} superconductors. *Phys. Rev. B* **79**, 014519 (2009).
- [S10] Tapp, J. H., Tang, Z. J., Lv, B., Sasmal, K., Lorenz, B.,

- Chu, P. C. W. & M. Guloy, A. M. LiFeAs: an intrinsic FeAs-based superconductor with $T_c = 18\text{K}$. *Phys. Rev. B* **78**, 060505(R) (2008).
- [S11] Parker, D. R., Pitcher, M. J., Baker, P. J., Franke, I., Lancaster, T., Blundell, S. J. & Clarke, S. J. Structure, antiferromagnetism and superconductivity of the layered iron arsenide NaFeAs. *Chem. Commun.*, 2009, 2189-2191.
- [S12] Johrendt, D. & Poettgen, R. Superconductivity, magnetism and crystal chemistry of $\text{Ba}_{1-x}\text{K}_x\text{Fe}_2\text{As}_2$. *Physica C* **469**, 332-339 (2009).
- [S13] Rotter, M., Tegel, M., Johrendt, D., Schellenberg, I., Hermes, W., & Pöttgen, R. Spin-density-wave anomaly at 140 K in the ternary iron arsenide BaFe_2As_2 . *Phys. Rev. B* **78**, 020503(R) (2008).
- [S14] Kamihara, Y., Watanabe, T., Hirano, M. & Hosono, H. Iron-based layered superconductor $\text{La}[\text{O}_{1-x}\text{F}_x]\text{FeAs}$ ($x = 0.05\text{-}0.12$) with $T_c = 26\text{ K}$. *J. Amer. Chem. Soc.* **130**, 3296-3297 (2008).
- [S15] Nomura, T., Inoue, Y., Matsuishi, S., Hirano, M., Kim, J. E., Kato, K., Takata, M., & Hosono, H. Comparison of crystal structures and effects of Co substitution in a new member of Fe-1111 superconductor family AeFeAsF ($\text{Ae} = \text{Ca}$ and Sr): a possible candidate for higher T_c superconductor. *Supercond. Sci. Technol.* **22**, 055016 (2009).
- [S16] Tegel, M., Johansson, S., Weiss, V., Schellenberg, I., Hermes, W., Poettgen, R. & Johrendt, D. Synthesis, crystal structure and spin-density-wave anomaly of the iron arsenide-fluoride SrFeAsF . *Europhys. Lett.* **84**, 67007 (2008).
- [S17] Tegel, M., Rotter, M., Weiss, V., Schappacher, F. M., Poettgen, R. & Johrendt, D. Structural and magnetic phase transitions in the ternary iron arsenides SrFe_2As_2 and EuFe_2As_2 . *J. Phys.: Condens. Matter* **20**, 452201 (2008).
- [S18] Wu, G., Chen, H., Wu, T., Xie, Y. L., Yan, Y. J., Liu, R. H., Wang, X. F., Ying, J. J. & Chen, X. H. Different resistivity response to spin density wave and superconductivity at 20 K in $\text{Ca}_{1-x}\text{Na}_x\text{Fe}_2\text{As}_2$. *J. Phys.: Condens. Matter* **20**, 422201 (2008).
- [S19] Kamihara, Y., Hiramatsu, H., Hirano, M., Kawamura, R., Yanagi, H., Kamiya, T. & Hosono, H. Iron-based layered superconductor: LaOFeP . *J. Am. Chem. Soc.* **128**, 10012-10013 (2006).
- [S20] Kutepov, A., Haule, K., Savrasov, S. Y. & Kotliar, G. Self consistent GW determination of the interaction strength: application to the iron arsenide superconductors. *Phys. Rev. B* **82**, 045105 (2010).
- [S21] Yin, Z. P., Haule, K. & Kotliar, G. Magnetism and charge dynamics in iron pnictides. *Nat. Phys.* **7**, 294-297 (2011).
- [S22] Shim, J. H., Haule, K., & Kotliar, G. Fluctuating valence in a correlated solid and the anomalous properties of δ -plutonium. *Nature* **446**, 513-516 (2007).
- [S23] Aichhorn, M., Biermann, S., Miyake, T., Georges, A. & Imada, M. Theoretical evidence for strong correlations and incoherent metallic state in FeSe. *Phys. Rev. B* **82**, 064504 (2010).
- [S24] Perdew, J. P. & Wang, Y. Accurate and simple analytic representation of the electron-gas correlation energy. *Phys. Rev. B* **45**, 13244-13249 (1992).
- [S25] Perdew, J. P., Burke, K. & Ernzerhof, M. Generalized gradient approximation made simple. *Phys. Rev. Lett.* **77**, 3865-3868 (1996).
- [S26] Hansmann, P., Arita, R., Toschi, A., Sakai, S., Sangiovanni, G. & Held, K. Dichotomy between large local and small ordered magnetic moment in iron-based superconductors. *Phys. Rev. Lett.* **104**, 197002 (2010).
- [S27] Hu, W. Z., Li, G., Zheng, P., Chen, G. F., Luo, J. L. & Wang, N. L. *Phys. Rev. B* **80**, 100507(R) (2009).
- [S28] Hu, W. Z., Dong, J., Li, G., Li, Z., Zheng, P., Chen, G. F., Luo, J. L. & Wang, N. L. Origin of the spin density wave instability in AFe_2As_2 ($\text{A}=\text{Ba}, \text{Sr}$) as revealed by optical spectroscopy. *Phys. Rev. Lett.* **101**, 257005 (2008).
- [S29] Chen, Z. G., Yuan, R. H., Dong, T. & Wang, N. L. Optical spectroscopy study on single crystalline LaFeAsO . *Phys. Rev. B* **81**, 100502(R) (2010).
- [S30] Qazilbash, M. M., Hamlin, J. J., Baumbach, R. E., Zhang, L. J., Singh, D. J., Maple, M. B. & Basov, D. N. Electronic correlations in the iron pnictides. *Nat. Phys.* **5**, 647-650 (2009).
- [S31] Moeller, G., Si, Q., Kotliar, G., Rozenberg, M. & Fisher, D. S. Critical behavior near the Mott transition in the Hubbard model. *Phys. Rev. Lett.* **74**, 2082-2085 (1995).
- [S32] Okada, I. & Yosida, K. Singlet ground state of the localized d -electrons coupled with conduction electrons in metals. *Progress of Theoretical Physics* **49**, 1483-1502 (1973).
- [S33] Ishida, H. & Liebsch, A. Fermi-liquid, non-Fermi-liquid, and Mott phases in iron pnictides and cuprates. *Phys. Rev. B* **81**, 054513 (2010).